Electrical and optical simulation of perovskite/silicon tandem solar cells using Tcad-Sentaurus

Cham Thi Trinh[1], Amran Al-Ashouri[2], Lars Korte[2], Daniel Amkreutz[1], Steve Albrecht[2], Bernd Stannowski[1] and Rutger Schlatmann[1]

1.PVcomB, Helmholtz-Zentrum Berlin für Materialien und Energie (HZB), Berlin 12489, Germany.
2.Young Investigator Group Perovskite Tandem Solar Cells, Helmholtz-Zentrum Berlin, 12489 Berlin, Germany.

***Abstract*—This work focuses on 2D device simulation for perovskite/tandem solar cells, aiming to reproduce the experimental current-voltage curves and to explore further steps for efficiency improvements. The results demonstrate that a reasonable J-V curve can be obtained when the indium tin oxide (ITO) layer that interconnects both subcells is treated as either a semiconductor or conductor. In both cases, band to band tunneling and/or additional built-in voltage governed by proper work functions of ITO and tin oxide (SnOx) films are required to obtain the high experimental FFs of >80%. Optical and electrical losses in the tandem device are also addressed by quantum efficiencies (EQE, IQE) and reflectance simulation.**

Keywords—Perovskite/Silicon tandem, simulation, Tcad-Sentaurus, band to band tunneling, built-in voltage

I. Introduction

Perovskite-based solar cells have gained high attention in the photovoltaic community in recent years. This is not only due to high power conversion efficiencies with simple and cost-effective fabrication processes, but also because they are a perfect tandem partner with the band gap tunability, as well as process compatibility to silicon and copper-indium-gallium-selenide (CIGSe) technologies [1], [2]. The rapid increase in the efficiency of both single and tandem-based perovskite solar cells indicates the potential of these emerging materials. An efficiency as high as 25.6 % was reported for the best perovskite single cell [3] and the current record perovskite/silicon tandem cell has reached 29.52 % as demonstrated by Oxford PV [4]. As efficiencies approach practical limits, a better understanding of the device physics and proper loss analyses will become more important. This work focuses on the modeling of tandem solar cells using the TCAD-Sentaurus simulation tool [5]. The device structure in this study is based on the currently best published perovskite tandem cell with certified value of 29.2% [6], which employed a self-assembled monolayer (SAM) as the hole-selective layer. Most important result of this simulation approach was to identify present limitations and how to enhance charge extraction, particularly at the hole transport layer/indium tin oxide (ITO) interface of the perovskite cell [7], [8]. It is reported in some simulation literatures that the built-in potential, which is originated from different work functions of contacts [7], [9] or offset between contact/transport layers [10] is needed to avoid carrier accumulation at transport layers, thus, enabling sufficient carrier collection through transport layers. These works suggest the important role of ITO's properties in cell performance. In this study, the ITO layer was treated as either a semiconductor or conductor to investigate the possible physical models to simulate J-V curves. In both cases, a built-in potential created from the difference of work functions (WFs) of the conductive layers was necessary to model fill factors (FFs) higher than 70%. If the ITO was treated as a semiconductor, band-to-band tunneling had to be included in the model to enable charge carrier transport at the SAM/ITO interface. The experimental J-V curves of the tandem device [6] could be reproduced by the simulation with both the semiconducting and conducting ("quasi-metallic") ITO approaches. Finally, external and internal quantum efficiency (EQE and IQE) and optical reflection (R) simulations were done to estimate the loss in the cell.

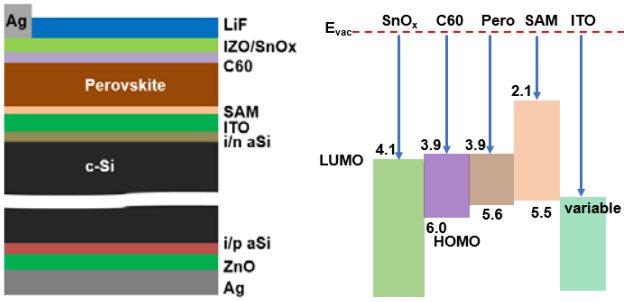

Fig. 1. Simulated device scheme (left) and energetic alignment (right) of the top cell.

II. Siimulated devices

The simulated devices mimic the same material configuration and include all layers with the same thicknesses as in the experimental cell [6], except for the LiF interlayer at the C60/perovskite interface. The thickness of SAM was assumed to 1 nm. The complex refractive index (n,k) data of the layers was calculated from measured spectral ellipsometry data for the films. Input parameters for perovskite cell simulation are listed in Table I. The band gap of the perovskite film was set as measured value (1.68 eV) of the real cell [6]. The value of effective density of states (4.5×10^{18} cm^{-3}) and the radiative recombination rate (3×10^{11} cm^{-3}/s) of perovskite film were chosen to obtain the experimental value of the dark saturation current J_0 (3×10^{-22} mA/cm^{-2}), the corresponding radiative

TABLE I. INPUT PARAMETERS FOR PEROVSKITE CELL.

Parameters	SnO_x	C60	Pero	SAM	ITO
Band gap (eV)	3.5	2.1	1.68	2.1	3.72
Electron affinity (eV)	4.1	3.9	3.9	5.5	variable
Doping concentration (cm^{-3})	1×10^{20}	1×10^{5}	1×10^{10}	1×10^{5}	1×10^{20}
Bulk lifetime (µs)	x	1×10^{-3}	1	1×10^{-3}	x
Electron / Hole mobilities ($cm^2V^{-1}s^{-1}$)	50/30	1×10^{-3}/ 1×10^{-2}	6/24	1×10^{-3}	50/30
Effective density state (cm^{-3})	3×10^{18}	1×10^{21}	4.5×10^{18}	1×10^{21}	1×10^{18}
Dielectric constant	3.3	5	22	3.5	3.3

voltage limit is 1.36 V. Carrier lifetime and mobilities were taken from experimental values measured on the perovskite film [6], [11]. Transport layers were kept as non-doped materials. The interface state density at perovskite/transport layers are set at 2×10^{11} cm^{-2} to get Voc of 1.2 V for the perovskite cell. Most critical parameters to fit with our model are FF values as in the experimental range, i.e. 75-85 % for FF. Illuminated spectrum for single cells were adjusted to match the experimental Jsc of tandem cell (19.3 mA/cm^2). Fig. 1 shows the energetic alignment of the layers comprising the cell. All values for the SAM, C60 and Perovskite were taken from the literature [6].

For optical simulation, a transfer matrix method was used to solve optical absorption in the layers. Surface roughness scattering model with the root mean square roughness of 2.5 µm was implemented to Si back surface to enhance light trapping at long wavelengths of the tandem cell. Monochromatic light sources with signal intensity of 0.01 W/cm^2 was used for EQE simulation. Additional bias light (am1.5g solar spectrum) was assumed to adjust the excess carrier density to similar levels as in the EQE experiments. IQE is calculated as the ratio of EQE and (1-R).

III. RESULTS AND DISSCUSION

A. *Top cell*

1) ITO treated as semiconductor

When ITO is treated as a semiconductor, the experimental J-V curve can be reproduced if:

- Suitable band alignment is achieved: The HOMO level of SAM is lower than the valence band of ITO, as shown as dot lines in Fig. 2.
- Band-to-band tunneling is activated for charge carrier transport at the SAM/ITO interface.
- Built-in voltage is added by increasing WF_{ITO} to avoid otherwise low simulated FF, as shown in Fig. 3.

Suitable band alignment for band to band tunneling is shown as the red dotted lines in figure 2. In case of band misalignment, the HOMO level of SAM is below conduction band level of ITO and holes can't travel to the ITO, resulting in convergence problems in the simulation. Fig. 3 shows the

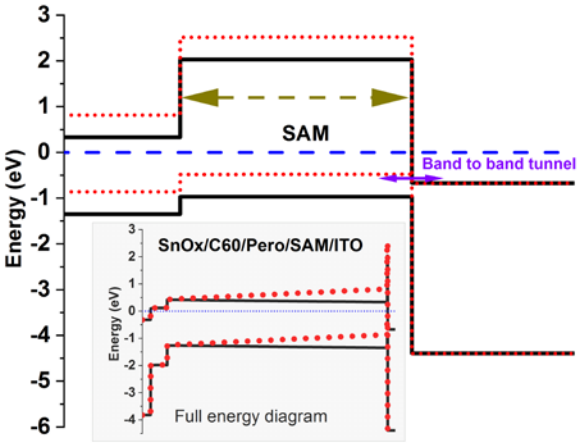

Fig. 2. Energy band diagram at the Pero/SAM/ITO junction at dark equilibrium conditions for the case of proper band alignment (red dot lines) or misaligned bands (black solid lines). The insert figure is the band diagram for the complete device.

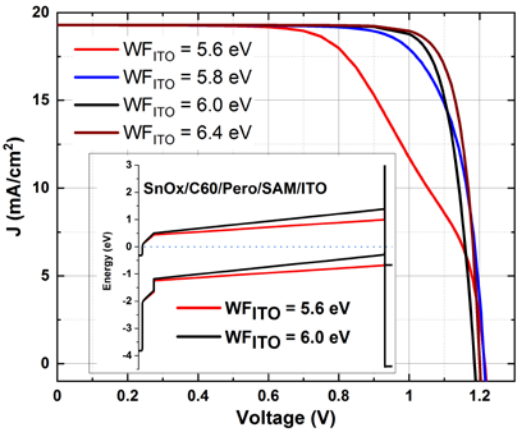

Fig. 3. The influence of built-in voltages on cell performance. WF_{ITO} varies from 5.6-6.4 eV and WF_{SnOx} is 4.1 eV. Inset figure shows the band diagram for low and high built-in voltages at equilibrium condition in the dark.

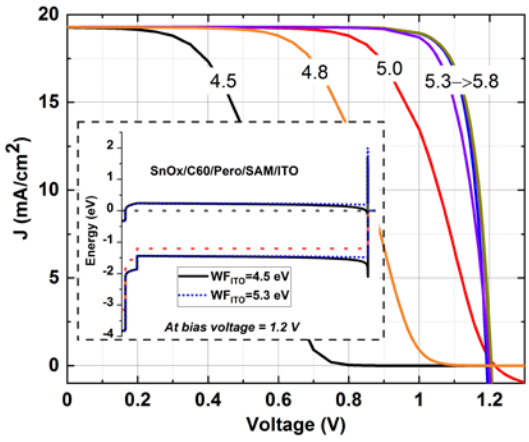

Fig. 4. Simulated J-V curves at variation of WF_{ITO}. Inset figure are the band diagrams of the cell at bias voltage of 1.2 V under illumination for WF_{ITO} of 4.5 and 5.3 eV. WF_{SnOx} is 4.1 eV.

influence of the built-in voltage (calculated as the difference of WF_{ITO} and WF_{SnOx}) on FF performance of the cell. Band diagrams of the cell at WF_{ITO} of 5.6 and 6.0 eV are plotted in the inset of figure 3. One can see a higher built-in potential

TABLE 1. EXPERIMENTAL AND SIMULATED CELL PARAMETERS. VALUES FROM SIMULATED DEVICE ARE FOR ITO AS CONDUCTOR.

Devices		Jsc (mA/cm²)	Voc (V)	FF (%)	Eff (%)
Simulated/ *Experimental*	Pero Cell	19.3	1.21	79.6	18.6
	Si Cell	19.3/ *20.2*	0.71/ *0.71*	80.3/ *80.6*	11.0/ *11.6*
	Tandem	19.3/ *19.3*	1.92/ *1.90*	81.5/ *79.5*	30.2/ *29.2*

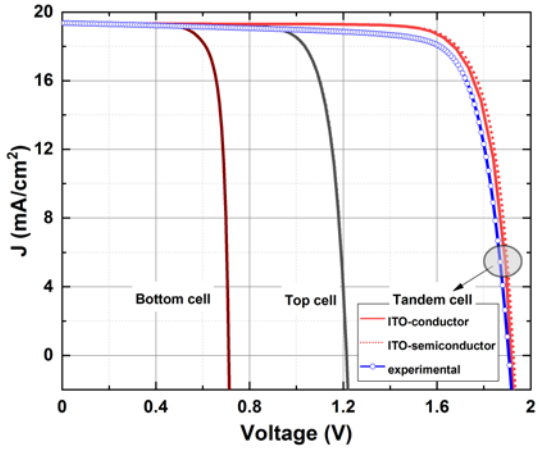

Fig. 5. Simulated J-V curves of single and tandem devices.

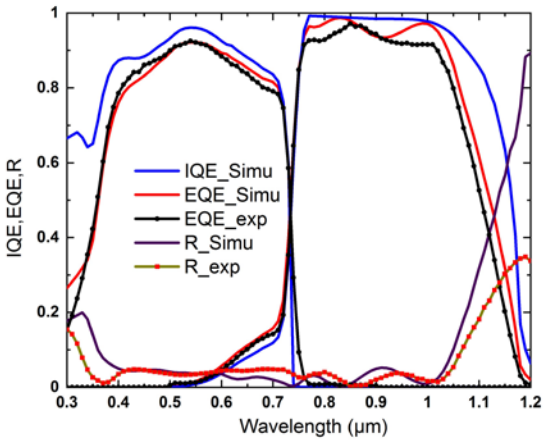

Fig. 6. Reflectance, EQE and IEQ of the simulated devices. EQE and R of the 29.2% efficiency cell are shown in comparison.

across the perovskite layer at higher WF_{ITO}, enhancing charge extraction. To raise the FF above 80 %, a high built-in voltage larger than 1.8 V is required. That means that the WF_{ITO} should be at least 5.9 eV which is quite high for this material even when a modified work function due to the SAM is considered [7].

2) ITO as a conductor

The cell performance when the ITO layer is implemented as a conductor was previously published [7]–[9]. In these simulations, the built-in potential originated from different work functions of electrodes is needed to overcome current blocking and achieve high FFs. As shown in the inset figure in figure 4, at low or no built-in voltage, energy bands bend downward at SAM/ITO interface, resulting in accumulation of electrons at the hole transport layer and current blocking, as seen in the simulated J-V curves in figure 4. A built-in voltage larger than 1.2 V is required to obtain a high FF above 80 %. Compared to the lowest limit of value of WF_{ITO} used when ITO is treated as semiconductor (5.9 eV as mentioned above), a WF_{ITO} of 5.3 eV is more resonable.

B. Bottom cell

The bottom cell is simulated to match the experimental data as well [6]. The nc-SiO_x film is described as a-Si:H(n) film with optical n,k data as measured for nc-SiO_x. The simulated device stack is ITO/aSi(n/i)/Si/aSi(i/p)/ZnO/Ag. Input parameters for Si cell are listed in the literature [12]. In this simulation, ZnO is used as a semiconductor material. Band to band tunneling was activated at the aSi(p)/ZnO interface. More detail in using band to band tunneling to simulate current transport at a doped aSi film/ transparent conductive oxide (TCO) was reported in the literature [13], [14].

C. Tandem cell

Fig. 5 shows the device performance for both simulation approaches used the ITO, i.e. semiconducting or "quasi-metallic". The simulated J-V curves match well the with experimental curve. The FF of the tandem cell is even higher than that of single cells [15]. An analysis of the overall resistance loss should be done to evaluate the FF values of the tandem cell. Fig. 6 shows simulated reflectance and quantum efficiency of the simulated device and the real cell. EQE of the top cell is in good agreement with experimental data. For the bottom cell, there is a mismatch in EQE and R, because of the losses from plasmon absorption or/and the real surface morphology of the back side were not implemented in this simulation.

IV. CONCLUSION

We establish suitable electrical models to simulate perovskite/silicon tandem devices, in which non-doped transport layers and a thin self-assembled monolayer were taken into simulation. The simulated J-V curves are in good match with experimental data. For non-doped transport layers, band to band tunneling and built-in potential originated from the choice of suitable work functions of conductive transport layers, which play important roles on charge carrier selection, thus, enhancing FF. In the scope of this simulation, it is suitable to treat the ITO as conductor, rather than as a semiconductor, to match modelled FF to the experimental range. Further works on adjusting the defect density at the interfaces and in the bulk of the perovskite as well as back-side texture/light trapping should be a focus in order to get better match between experimental and simulated results.

ACKNOWLEDGMENT

The authors would like to thank Prof. Thomas Kirchartz (Forschungszentrum Jülich GmbH), Prof. Reiner Klenk (Helmholtz-Zentrum Berlin GmbH) and Dr. Nga T. T. Phung (Eindhoven University of Technology) for interesting discussions.

REFERENCES

[1] M. Jošt, L. Kegelmann, L. Korte, and S. Albrecht, "Monolithic Perovskite Tandem Solar Cells: A Review of the Present Status and Advanced Characterization Methods Toward 30% Efficiency," *Advanced Energy Materials*, vol. 10, no. 26, p. 1904102, Jul. 2020, doi: 10.1002/aenm.201904102.

[2] E. Köhnen *et al.*, "Highly efficient monolithic perovskite silicon tandem solar cells: analyzing the influence of current mismatch on device performance," *Sustainable Energy Fuels*, vol. 3, no. 8, pp. 1995–2005, 2019, doi: 10.1039/C9SE00120D.

[3] "https://www.pv-magazine.com/2021/04/06/unist-epfl-claim-25-6-efficiency-world-record-for-perovskite-solar-cell/."

[4] "https://mercomindia.com/oxford-record-efficiency-perovskite-solar/."

[5] *Sentaurus Structure Editor User Guide*, Synopsis, Inc., Mountain View, CA, USA. 2011.

[6] A. Al-Ashouri *et al.*, "Monolithic perovskite/silicon tandem solar cell with >29% efficiency by enhanced hole extraction," *Science*, vol. 370, no. 6522, pp. 1300–1309, Dec. 2020, doi: 10.1126/science.abd4016.

[7] O. J. Sandberg *et al.*, "On the Question of the Need for a Built-In Potential in Perovskite Solar Cells," *Adv. Mater. Interfaces*, vol. 7, no. 10, p. 2000041, May 2020, doi: 10.1002/admi.202000041.

[8] T. Kirchartz, J. Bisquert, I. Mora-Sero, and G. Garcia-Belmonte, "Classification of solar cells according to mechanisms of charge separation and charge collection," *Phys. Chem. Chem. Phys.*, vol. 17, no. 6, pp. 4007–4014, 2015, doi: 10.1039/C4CP05174B.

[9] M. Stolterfoht *et al.*, "The impact of energy alignment and interfacial recombination on the internal and external open-circuit voltage of perovskite solar cells," *Energy Environ. Sci.*, vol. 12, no. 9, pp. 2778–2788, 2019, doi: 10.1039/C9EE02020A.

[10] T. Kirchartz, "High open-circuit voltages in lead-halide perovskite solar cells: experiment, theory and open questions," *Phil. Trans. R. Soc. A.*, vol. 377, no. 2152, p. 20180286, Aug. 2019, doi: 10.1098/rsta.2018.0286.

[11] A. Al-Ashouri *et al.*, "Conformal monolayer contacts with lossless interfaces for perovskite single junction and monolithic tandem solar cells," *Energy Environ. Sci.*, vol. 12, no. 11, pp. 3356–3369, 2019, doi: 10.1039/C9EE02268F.

[12] C. T. Trinh *et al.*, "Assessment of Bulk and Interface Quality for Liquid Phase Crystallized Silicon on Glass," *IEEE Journal of Photovoltaics*, vol. 9, no. 2, pp. 364–373, Mar. 2019, doi: 10.1109/JPHOTOV.2018.2889183.

[13] P. Procel, G. Yang, O. Isabella, and M. Zeman, "Theoretical evaluation of contact stack for high efficiency IBC-SHJ solar cells," *Solar Energy Materials and Solar Cells*, vol. 186, pp. 66–77, Nov. 2018, doi: 10.1016/j.solmat.2018.06.021.

[14] Y. Abdulraheem, M. Ghannam, H. S. Radhakrishnan, and I. Gordon, "The Role of Silicon Heterojunction and TCO Barriers on the Operation of Silicon Heterojunction Solar Cells: Comparison between Theory and Experiment," *International Journal of Photoenergy*, vol. 2021, pp. 1–12, Mar. 2021, doi: 10.1155/2021/6632180.

[15] M. Boccard and C. Ballif, "Influence of the Subcell Properties on the Fill Factor of Two-Terminal Perovskite–Silicon Tandem Solar Cells," *ACS Energy Lett.*, vol. 5, no. 4, pp. 1077–1082, Apr. 2020, doi: 10.1021/acsenergylett.0c00156.